Chemical Science

EDGE ARTICLE

View Article Online
View Journal | View Issue

Cite this: *Chem. Sci.*, 2018, **9**, 5087

The robust, readily available cobalt(III) trication $[Co(NH_2CHPhCHPhNH_2)_3]^{3+}$ is a progenitor of broadly applicable chirality and prochirality sensing agents†

Quang H. Luu, Kyle G. Lewis,‡ Anik Banerjee, Nattamai Bhuvanesh and John A. Gladysz *

When NMR spectra of chiral racemic organic molecules containing a Lewis basic functional group are recorded in the presence of air and water stable salts of the cobalt(III) trication $[Co((S,S)\text{-}NH_2CHPhCHPhNH_2)_3]^{3+}$ ($\mathbf{2}^{3+}$), separate signals are usually observed for the enantiomers (28 diverse examples, >12 functional groups). Several chiral molecules can be simultaneously analyzed, and enantiotopic groups in prochiral molecules differentiated (16 examples). Particularly effective are the mixed bis(halide)/tetraarylborate salts $\Lambda\text{-}\mathbf{2}^{3+}$ $2X^-BAr_f^-$ (X = Cl, I; BAr_f = $B(3,5\text{-}C_6H_3(CF_3)_2)_4$), which are applied in CD_2Cl_2 or $CDCl_3$ at 1–100 mol% (avg 34 and 14 mol%). Job plots establish 1 : 1 binding for $\Lambda\text{-}\mathbf{2}^{3+}$ $2Cl^-BAr_f^-$ and 1-phenylethyl acetate (**4**) or 1-phenylethanol (**10**), and *ca.* 1 : 2 binding with DMSO (CD_2Cl_2). Selected binding constants are determined, which range from 7.60–2.73 M^{-1} for the enantiomers of **10** to 28.1–22.6 M^{-1} for the enantiomers of **4**. The NH moieties of the C_2 faces of the trication are believed to hydrogen bond to the Lewis basic functional groups, as seen in the crystal structure of a hexakis(DMSO) solvate of $\Lambda\text{-}\mathbf{2}^{3+}$ $3I^-$. These salts rank with the most broadly applicable chirality sensing agents discovered to date.

Received 3rd April 2018
Accepted 9th May 2018

DOI: 10.1039/c8sc01510d

rsc.li/chemical-science

1. Introduction

Ever since the recognition of molecular chirality, chemists have sought to quantify enantiomer ratios in non-racemic samples.[1] For more than a century, the dominant method was polarimetry, despite many intrinsic limitations.[2,3] Today, nearly every analytical technique is being brought to bear on the problem, often in a quest for high throughput screening.[4,5] Two broad classes of assays see the most use: "chiral" chromatography[6,7] and NMR spectroscopy.[8–13]

NMR methods can be divided into three principal categories: chiral derivatizing agents (CDAs),[8–12,14,15] paramagnetic chiral lanthanide shift reagents (CLSRs),[16] and chiral solvating agents (CSAs).[8,10–13] Over the past few years, the last approach has attracted increasing attention.[17–30] Many but not all of the CSAs are hydrogen bond donors, often with two-four NH or OH groups.[17,21,22,25–28,30] Some of these have been tailored to recognize a specific functional group,[19,23,24,26–28] while others have wider applicability.[17,20–22,25,29,30]

The first chiral inorganic compounds to be isolated in enantiomerically pure form were reported by Werner some 105 years ago, and included salts of the trication $[Co(en)_3]^{3+}$ ($\mathbf{1}^{3+}$; en = ethylenediamine).[31–35] We have recently found that lipophilic salts of this trication[36] and the related species $[Co((S,S)\text{-}NH_2CHArCHArNH_2)_3]^{3+}$ ($\mathbf{2}^{3+}$ for Ar = Ph)[37–39] and $[Co(en)_2(NH_2CH_2CH((CH_2)_nN(CH_3)_2)NH_2)]^{3+}$ ($\mathbf{3}^{3+}$)[40] – all of which are depicted in Fig. 1 – serve as hydrogen bond donor catalysts for a variety of organic transformations. The trication $\mathbf{1}^{3+}$ features only metal centered chirality, for which the absolute configurations are traditionally designated Λ and Δ.[41] In the trications $\mathbf{2}^{3+}$ and $\mathbf{3}^{3+}$, the three ethylenediamine ligands are substituted with six aryl groups[42] or a single $(CH_2)_nN(CH_3)_2$ moiety, respectively.[43] The latter constitutes a bifunctional catalyst.[40] Both enantiomers of the $NH_2CHPhCHPhNH_2$ (dpen) ligand in $\mathbf{2}^{3+}$ are commercially available at modest prices.[44]

Although the mechanisms of these transformations are still under investigation, their effectiveness is thought to be rooted in the large number of NH groups (twelve). Those of one diastereomer of $\mathbf{2}^{3+}$ are depicted in Fig. 1 (bottom). As many as five to six might play a role in transition state assemblies,[45] as opposed to a maximum of two with most literature catalysts such as thioureas.[46] As such, they might possess unique

Department of Chemistry, Texas A&M University, P.O. Box 30012, College Station, Texas 77842-3012, USA. E-mail: gladysz@mail.chem.tamu.edu

† Electronic supplementary information (ESI) available: CCDC 1812259. For ESI and crystallographic data in CIF or other electronic format see DOI: 10.1039/c8sc01510d

‡ Present address: Synthetics Technology, ExxonMobil Chemical Company, 4500 Bayway Drive, Baytown, TX 77520.

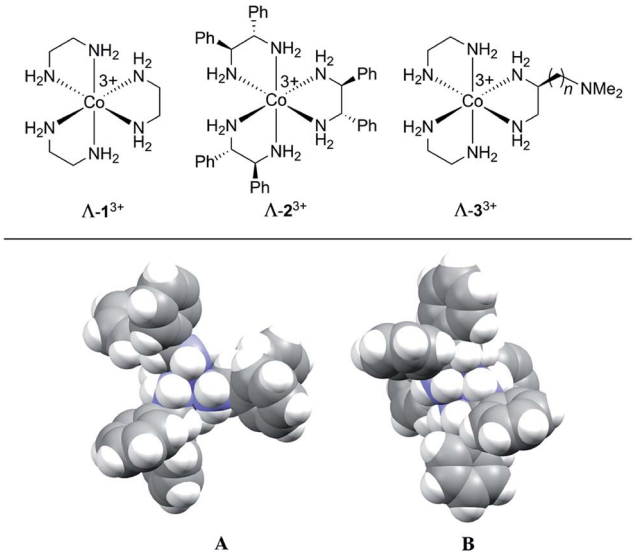

Fig. 1 (Top) Chiral hydrogen bond donor catalysts based upon cobalt(III) tris(ethylenediamine) trications. (Bottom) Space filling representations of the trication of Λ-2^{3+} $3Cl^- \cdot 2H_2O \cdot 2CH_3OH$; **A**, view down the idealized C_3 axis; **B**, view down one of three idealized C_2 axes.[42]

capabilities as CSAs. Indeed, in the course of screening catalytic reactions by NMR, marked differentiation of enantiomers and enantiotopic (prochiral) groups were noted.

In this paper, we report a detailed study of chirality and prochirality sensing by the preceding complexes, and in particular the commercially available[47] bis(chloride)/tetraarylborate mixed salt Λ-2^{3+} $2Cl^-BAr_f^-$ (BAr_f = B(3,5-$C_6H_3(CF_3)_2)_4$) and the bis(iodide) analog Λ-2^{3+} $2I^-BAr_f^-$. These robust, air and water stable substances are remarkable in affording baseline NMR signal separations at loadings as low as 1 mol%. The scope of functional group applicability ranks with the most versatile existing CSAs, and they appear unsurpassed in differentiating enantiotopic groups in achiral molecules.[48–55]

2. Results

2.1. Syntheses of cobalt(III) CSAs

Enantiopure Λ-1^{3+} $3BAr_f^-$ and diastereopure Λ-2^{3+} $2Cl^-BAr_f^-$, Λ-2^{3+} $2Cl^-B(C_6F_5)_4^-$, Λ-2^{3+} $3BAr_f^-$, and Δ-2^{3+} $2Cl^-BAr_f^-$ were prepared according to previously reported procedures.[36,42] Those for the BAr_f^- salts of Λ-2^{3+} are summarized in Scheme 1. The key precursor Λ-2^{3+} $3Cl^-$ is easily synthesized from $CoCl_2$ or $Co(OAc)_2$, O_2, and (*S*,*S*)-dpen.[42]

The new triiodide salt Λ-2^{3+} $3I^-$ was isolated in 97% yield from the reaction of Λ-2^{3+} $3Cl^-$ and KI in acetone.[56] Addition of 1.0 equiv. of Na^+ BAr_f^- afforded the mixed bis(iodide)/tetraarylborate salt Λ-2^{3+} $2I^-BAr_f^-$ in 99% yield after workup. This complex could also be isolated in >99% yield from the reaction of excess NaI and Λ-2^{3+} $2Cl^-BAr_f^-$. It possessed the advantage of being – unlike the other salts – soluble in the inexpensive deuterated solvent $CDCl_3$.

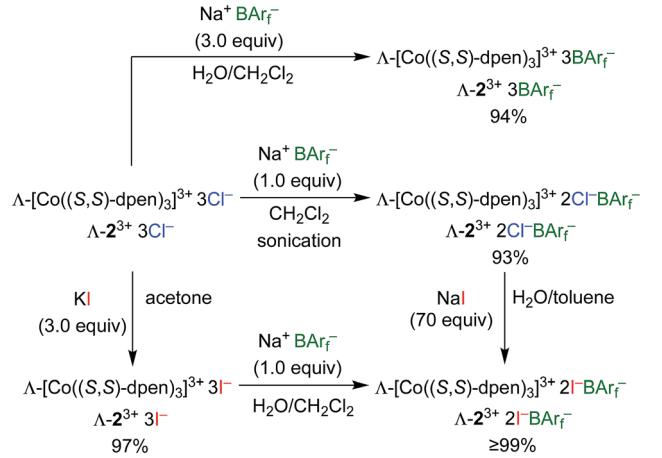

Scheme 1 Syntheses of cobalt(III) CSAs (all reactions at room temperature, 5 min to 6 h).

2.2. Screening of cobalt(III) CSAs

The efficacies of the preceding complexes as CSAs were screened with racemic 1-phenylethyl acetate (**4**). As presented in Table 1, 0.0071 M solutions of the CSAs in various solvents were combined with neat **4** (1.0 equiv.). In favorable cases, the chemical shifts of all of the aliphatic NMR signals of the enantiomers differed, as detailed in Table S1 of the ESI.† In all of these cases, the methine (PhC***H***$(CH_3)O(C{=}O)CH_3$) protons were the most strongly differentiated (Δδ, Table 1). However, Λ-1^{3+} $3BAr_f^-$ (entry 1) was ineffective in all assays, including additional analytes such as 1-phenethyl amine (**5**), phenyl methyl sulfoxide (**6**), and 2-carbomethoxycyclopentanone (**7**).

In contrast, the bis(chloride) tetraarylborate salts Λ-2^{3+} $2Cl^-BAr_f^-$ and Λ-2^{3+} $2Cl^-B(C_6F_5)_4^-$ gave widely separated methine proton signals in CD_2Cl_2 (entries 2 and 4; Δδ 1.37–1.32 ppm). The opposite diastereomer of the former, Δ-2^{3+} $2Cl^-BAr_f^-$, was much less effective (entry 3, Δδ 0.15 ppm).

Table 1 Separation of the methine proton ^{1}H NMR signals (Δδ, ppm) of the enantiomers of racemic 1-phenylethyl acetate (**4**) as a function of CSA (1.0 equiv.) and solvent[a]

Entry	CSA	Solvent	Δδ
1	Λ-1^{3+} $3BAr_f^-$	CD_2Cl_2	—[b]
2	Λ-2^{3+} $2Cl^-BAr_f^-$	CD_2Cl_2	1.32
3	Δ-2^{3+} $2Cl^-BAr_f^-$	CD_2Cl_2	0.15
4	Λ-2^{3+} $2Cl^-B(C_6F_5)_4^-$	CD_2Cl_2	1.37
5	Λ-2^{3+} $3BAr_f^-$	CD_2Cl_2	0.34
6	Λ-2^{3+} $2I^-BAr_f^-$	CD_2Cl_2	1.30
7	Λ-2^{3+} $2I^-BAr_f^-$	$CDCl_3$	1.75
8	Λ-2^{3+} $2I^-BAr_f^-$	Acetone-d_6	—[b]
9	Λ-2^{3+} $2I^-BAr_f^-$	CD_3CN	—[b]
10	Λ-2^{3+} $2I^-BAr_f^-$	DMSO-d_6	—[b]
11	Λ-2^{3+} $2Cl^-BAr_f^-$	Acetone-d_6	—[b]
12	Λ-2^{3+} $2Cl^-BAr_f^-$	CD_3CN	—[b]
13	Λ-2^{3+} $2Cl^-BAr_f^-$	DMSO-d_6	—[b]

[a] Samples were prepared in 5 mm NMR tubes as described in the Experimental section. [b] Separate signals for the enantiomers were not observed, although line widths increased from 0.6–0.9 to 1.0–2.0 Hz.

Interestingly, the corresponding tris(tetraarylborate) salt Λ-2^{3+} $3BAr_f^-$ was also less effective (entry 5; Δδ 0.34 ppm), despite the removal of all counter anions that can hydrogen bond to the NH groups of the trication.[42]

The bis(iodide) salt Λ-2^{3+} $2I^-BAr_f^-$ gave a high Δδ value (entry 6; 1.30 ppm), comparable to that of Λ-2^{3+} $2Cl^-BAr_f^-$. Happily, when Λ-2^{3+} $2I^-BAr_f^-$ was applied in the less polar and coordinating solvent $CDCl_3$, the Δδ value increased by 33% (entry 7, 1.75 ppm). Finally, when either Λ-2^{3+} $2Cl^-BAr_f^-$ or Λ-2^{3+} $2I^-BAr_f^-$ were employed in the more polar and coordinating solvents acetone-d_6, CD_3CN, or DMSO-d_6, the enantiomers of **4** were no longer differentiated (entries 8–13).

It was sought to establish the minimum CSA loading needed to resolve the NMR signals of the enantiomers. Accordingly, an NMR tube was charged with a 0.036 M CD_2Cl_2 solution of Λ-2^{3+} $2Cl^-BAr_f^-$ (0.70 mL, 0.025 mmol). Then neat **4** was added in increments (0.00050 mL; *ca.* 0.0012 g, 0.0050 mmol). As shown in Fig. 2, the Δδ values for all three aliphatic signals were plotted against the mol% of the CSA, which is in great excess at the start. The data spanned a range of 500 mol% down to 5 mol% (total volume of liquids: 0.7005 to 0.7500 mL, or less than a 7% concentration change). Although the Δδ values monotonically decreased, all signals maintained baseline separations.

The concentration dependence of the efficacies of the CSAs was also probed. For this purpose, a NMR tube was charged with a CD_2Cl_2 solution that was 0.040 M in **4** (0.020 mmol) and 0.010 M in Λ-2^{3+} $2Cl^-BAr_f^-$ (0.0050 mmol), or a CSA loading of 25 mol%. Then increments of CD_2Cl_2 were added, giving more dilute solutions. As shown in Fig. 3, there was little change in the Δδ values over a two fold dilution. However, up to a 30% decrease could be seen at the lower concentration ranges investigated.

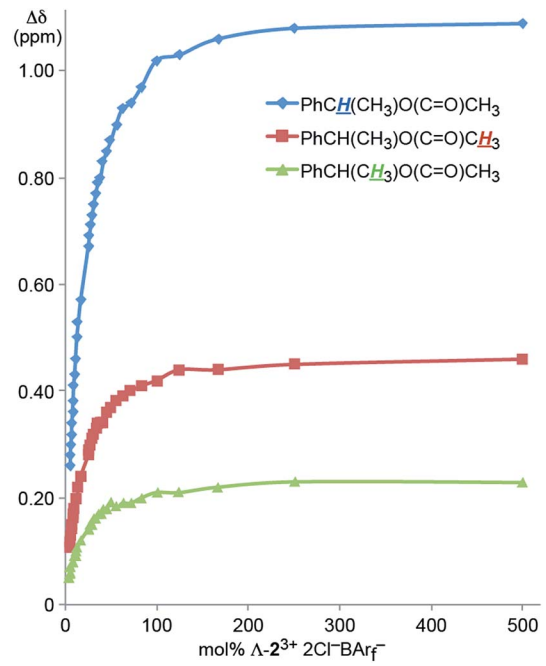

Fig. 2 Dependence of the separation of the aliphatic ^{1}H NMR signals of the enantiomers of **4** (Δδ, CD_2Cl_2) upon the mol% of the CSA Λ-2^{3+} $2Cl^-BAr_f^-$.

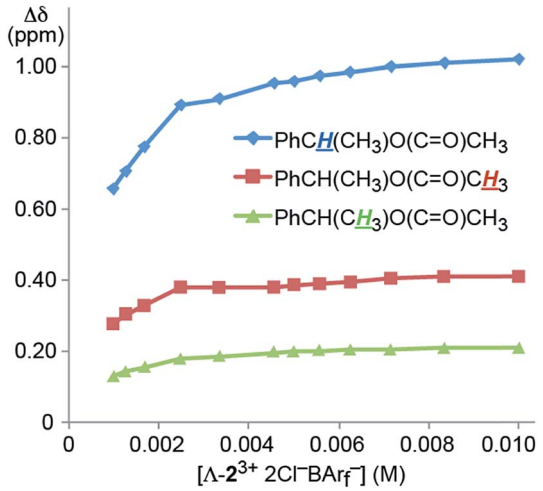

Fig. 3 Dependence of the separation of the aliphatic ^{1}H NMR signals of the enantiomers of **4** (Δδ, CD_2Cl_2) upon concentration using the CSA Λ-2^{3+} $2Cl^-BAr_f^-$ (constant at 25 mol%).

2.3. Functional group scope, chirality sensing

As summarized in Table 2, racemic chiral organic compounds with a variety of Lewis basic functionalities (**4–31**) were treated with the most effective CSAs, Λ-2^{3+} $2I^-BAr_f^-$ ($CDCl_3$ solution) and Λ-2^{3+} $2Cl^-BAr_f^-$ (CD_2Cl_2 solution). The former could differentiate the ^{1}H NMR signals of the enantiomers in every case, and the latter failed with only three analytes. The signals employed are denoted in red in Table 2. With fluorine (**15**) or phosphorus (**19**, **20**) containing analytes, $^{19}F\{^1H\}$ or $^{31}P\{^1H\}$ NMR was used instead. In cases where signals have been assigned to specific enantiomers, the samples were spiked with 0.50 equiv. of an authentic sample of one of the enantiomers.

With Λ-2^{3+} $2Cl^-BAr_f^-$, the loadings required for baseline to near-baseline signal separations ranged from 1 to 100 mol%, with an average of 34 mol%. With Λ-2^{3+} $2I^-BAr_f^-$, the loading range was identical, but the average decreased to 14 mol%. It was sought to verify that reliable quantitative data could be obtained from this new class of CSAs. Thus, scalemic samples of **4** were prepared and the ee values assayed using both Λ-2^{3+} $2Cl^-BAr_f^-$ and chiral HPLC, as described in the Experimental section. As depicted in Fig. S1 (ESI†), the two methods were essentially in perfect agreement.

When a chiral arene lacking a Lewis basic functional group, *sec*-butyl benzene ($PhCH(CH_3)CH_2CH_3$), was similarly investigated (Λ-2^{3+} $2I^-BAr_f^-$, $CDCl_3$), only a single set of (broadened) NMR signals was observed. Other analytes that gave only one set of signals included the benzylic chloride 1-phenyl-1-chloroethane, BINOL and its diacetate, and (surprisingly) the amide 5-hydroxymethyl-2-pyrrolidinone. However, the enantiomers of alkyl halides that contained additional Lewis basic functional groups, such as **29** and **30** (Table 2), were easily differentiated.

Table 2 Separation of key NMR signals of the enantiomers of various analytes in the presence of the CSAs Λ-2^{3+} $2I^-BAr_f^-$ ($CDCl_3$) or Λ-2^{3+} $2Cl^-BAr_f^-$ (CD_2Cl_2)[a]

Analyte/NMR signals[b]	$\Delta\delta^c$, mol%	$\Delta\delta^d$, mol%	Analyte/NMR signals[b]	$\Delta\delta^c$, mol%	$\Delta\delta^d$, mol%
4 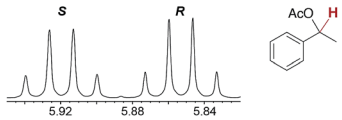	0.07, 1.0	0.29, 5.0	5 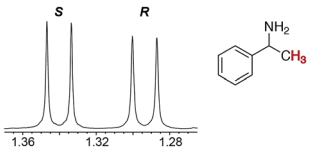	0.05, 0	0.01, 10
6 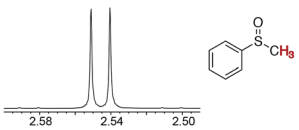	0.01, 4.0	0.05, 10	7 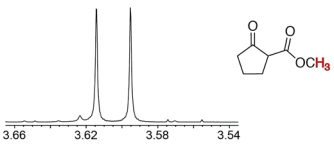	0.01, 3.0	0.05, 10
8 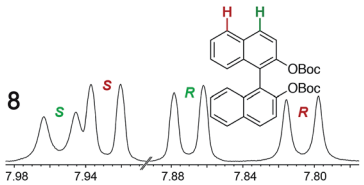	0.08, 100	0.04, 20	9 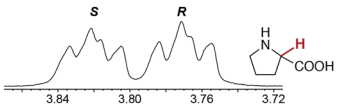	0.05, 20	0.04, 50
10 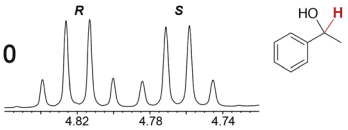	0.06, 3.0	0.07, 50	11 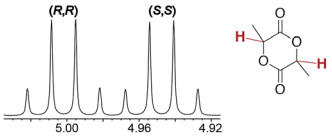	0.05, 3.0	0.06, 30
12 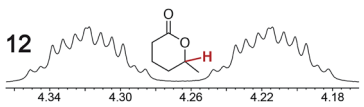	0.10, 1.0	0.43, 100	13 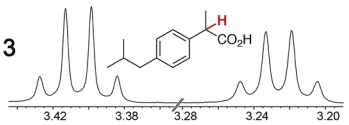	0.18, 30	0.06, 100
14 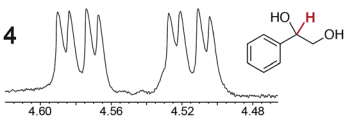	0.06, 30	0.32, 100	15 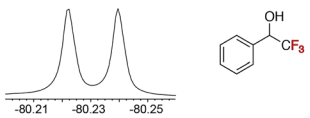	0.02[e], 30	0.04[e], 100
16 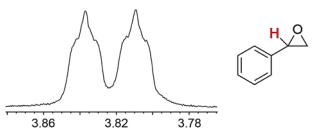	0.03, 10	0.04, 4.0	17 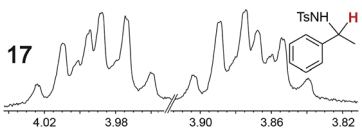	0.12, 30	0.28, 100
18 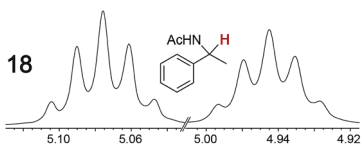	0.11, 1.0	0.09, 1.0	19 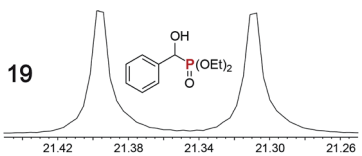	0.09[f], 11	0.07[f], 10
20 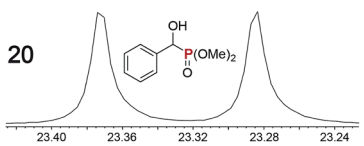	0.09[f], 3.0	0.10[f], 2.0	21 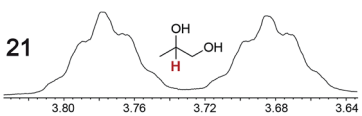	0.09, 5.0	0.09, 12
22 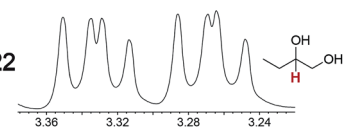	0.06, 5.0	0.06, 4.0	23 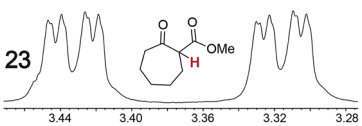	0.11, 7.0	0.16, 50
24 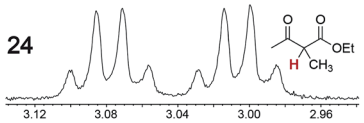	0.07, 33	—[g]	25 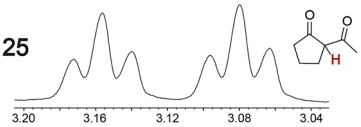	0.08, 6.0	0.05, 33

Table 2 (*Contd.*)

Analyte/NMR signals[b]	$\Delta\delta^c$, mol%	$\Delta\delta^d$, mol%	Analyte/NMR signals[b]	$\Delta\delta^c$, mol%	$\Delta\delta^d$, mol%
26 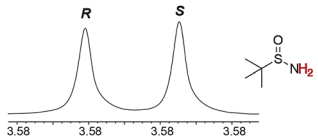	0.05, 2.0	0.06, 3.0	**27** 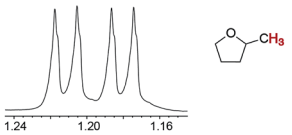	0.03, 3.0	—[g]
28 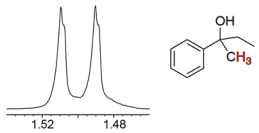	0.02, 22	—[g]	**29** 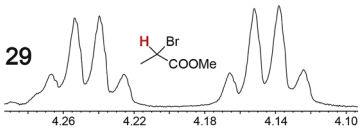	0.10, 11	0.07, 25
30 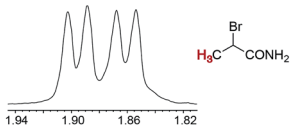	0.04, 2.0	0.04, 2.0	**31** 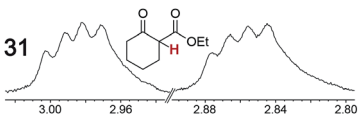	0.12, 18	0.06, 18

[a] Samples were prepared in 5 mm NMR tubes as described in the Experimental section. [b] The spectra depicted (^{1}H unless noted) were obtained with Λ-**2**$^{3+}$ 2I$^-$BAr$_f^-$ in $CDCl_3$. [c] Signal separation (ppm)/mol% using Λ-**2**$^{3+}$ 2I$^-$BAr$_f^-$. [d] Signal separation (ppm)/mol% using Λ-**2**$^{3+}$ 2Cl$^-$BAr$_f^-$. [e] ^{19}F{^{1}H} NMR spectra were utilized. [f] ^{31}P{^{1}H} NMR spectra were utilized. [g] Separate signals for the enantiomers were not observed.

2.4. Prochirality sensing

The types of experiments in the previous section were repeated with achiral molecules using a CSA loading of 100 mol% (1.0 equiv.). As summarized in Table 3, in many cases different signals were observed for enantiotopic groups. Enantiotopic geminal or vicinal hydrogen atoms also became coupled to each other. Achiral molecules in which enantiotopic groups were not differentiated include nitroethane, propionitrile, propionic acid, methyl isovalerate, tetrahydrofuran, and diethyl phosphite.

2.5. Enhanced throughput sensing

Higher throughput variants of the above methodology would be desirable. Thus, it was tested whether the enantiomeric purities of two or more analytes could be simultaneously determined. A $CDCl_3$ solution of racemic **4**, 2-carbomethoxycyclopentanone (**7**), 1-phenylethanol (**10**), and two hydroxyphenylmethyl dialkyl phosphonates (**19**, **20**) was prepared (2.0 : 2.0 : 2.0 : 1.0 : 2.0 mol ratio). Then Λ-**2**$^{3+}$ 2I$^-$BAr$_f^-$ was added (100 mol% with respect to **19**; 50 mol% with respect to the other analytes; average loading per analyte 11 mol%).

As shown in Fig. 4, the enantiomers of all five analytes were differentiated by NMR. Such experiments are potentially complicated by overlapping signals, but this is sidestepped in Fig. 4 by using a second nucleus, ^{31}P, to assay the phosphonates **19** and **20**. Some practical uses of simultaneous enantiomeric purity assays would include kinetic resolutions,[57–59] for example the acetylation of **10** to **4** or *vice versa*,[57–60] and enantioselective reactions that afford two or more diastereomers. To date, the closest approximation to this capability seems to involve covalent adducts of CDAs where all analytes contain a common functional group (*e.g.*, a primary amine).[61]

2.6. Mechanism of chirality and prochirality sensing

Some insight has been previously acquired regarding hydrogen bonding between the twelve NH protons of the trications **1**$^{3+}$ and **2**$^{3+}$ and various counter anions.[37,42,45] For example, data for Λ-**2**$^{3+}$ 2Cl$^-$BAr$_f^-$ indicate that the two chloride anions strongly bind to the two C_3 faces (Fig. 1, bottom left), shifting the ^{1}H NMR signals of six NH protons markedly downfield (*ca.* δ 8 ppm). The other six NH protons, which occupy the three C_2 faces (Fig. 1, bottom right), have only the solvent or the very poorly coordinating BAr$_f^-$ anion to interact with. Accordingly, their ^{1}H NMR signals remain upfield (*ca.* δ 4 ppm).[37] These trends are illustrated in the bottom spectrum in Fig. 5, although it deserves emphasis that the signal separation is both concentration and temperature dependent.[42]

As exemplified by the other spectra in Fig. 5, CD_2Cl_2 solutions of Λ-**2**$^{3+}$ 2Cl$^-$BAr$_f^-$ have been titrated with various analytes, such as dimethyl malonate, *trans*-β-nitrostyrene, methyl ethyl ketone, and both enantiomers of **4**. In proceeding from one to 10 equivalents, appreciable downfield shifts of the upfield C_2 NH signals are observed. The downfield C_3 NH signals are much less affected. Often there is virtually no shift, as seen with dimethyl malonate (Fig. 5, $\Delta\delta = 0.07$ ppm), *trans*-β-nitrostyrene, and methyl ethyl ketone; with the enantiomers of **4**, there is a modest upfield trend (0.13–0.33 ppm). Although these shifts may reflect a combination of phenomena, it seems assured that the donor functionalities in the analytes hydrogen bond to the C_2 faces.

Next, Job plots[62] were constructed using ^{1}H NMR data (CD_2Cl_2) for Λ-**2**$^{3+}$ 2Cl$^-$BAr$_f^-$ and the enantiopure analytes (*S*)-**4** and (*S*)-**10** as described in the Experimental section. As shown in Fig. 6, both exhibited maxima when the mol fraction of both components was 0.50, indicative of 1 : 1 adducts. Analogous experiments with the prochiral analyte DMSO showed

Table 3 Separation of ^{1}H NMR signals of enantiotopic groups of various achiral analytes in the presence of 100 mol% (1.0 equiv.) of the CSAs Λ-2^{3+} $2I^-BAr_f^-$ ($CDCl_3$) or Λ-2^{3+} $2Cl^-BAr_f^-$ (CD_2Cl_2)[a]

Analyte/NMR signals[b]	Δδ[c]	Δδ[d]	Analyte/NMR signals[b]	Δδ[c]	Δδ[d]
32 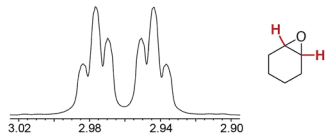	0.03	0.04	**33** 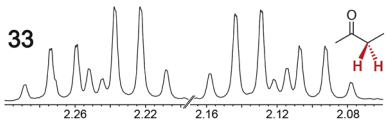	0.12	0.10
34 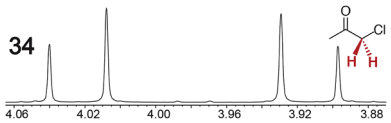	0.12	0.23	**35** 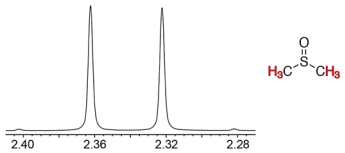	0.04	0.12
36 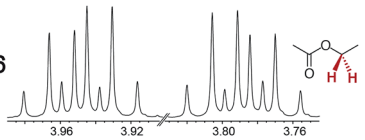	0.16	0.15	**37** 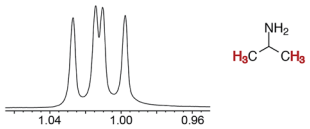	0.02	0.02
38 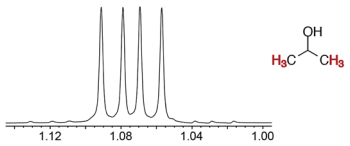	0.03	0.02	**39** 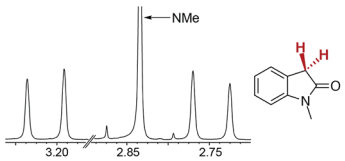	0.46	0.66
40 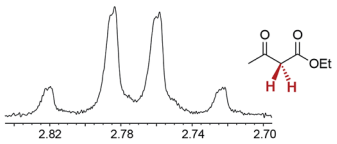	0.05	0.04	**41** 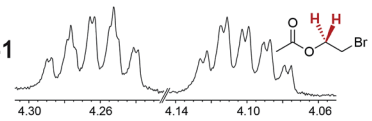	0.16	0.09
42 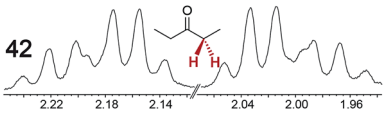	0.17	0.11	**43** 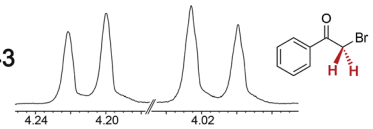	0.20	0.09
44 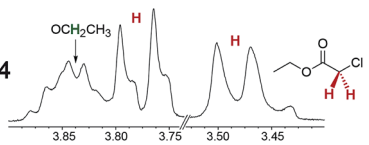	0.30	0.18	**45** 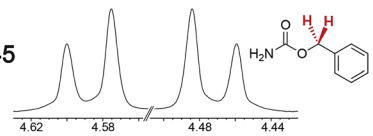	0.12	0.11
46 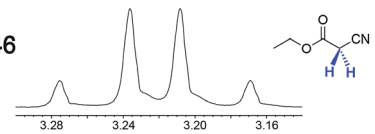	—[e]	0.07	**47** 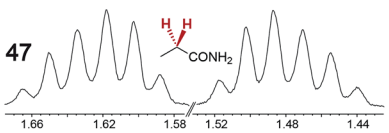	0.15	0.10

[a] Samples were prepared in 5 mm NMR tubes as described in the Experimental section. [b] The spectra depicted were obtained with Λ-2^{3+} $2I^-BAr_f^-$ in $CDCl_3$. [c] Signal separation (ppm) using Λ-2^{3+} $2I^-BAr_f^-$. [d] Signal separation (ppm) using Λ-2^{3+} $2Cl^-BAr_f^-$. [e] Separate signals for the enantiomers were not observed in the presence of 100–500 mol% of Λ-2^{3+} $2I^-BAr_f^-$.

a maximum when the mol fraction of the CSA was 0.3, indicative of a *ca.* 2 : 1 DMSO/Λ-2^{3+} $2Cl^-BAr_f^-$ adduct.

In an established protocol for obtaining binding constants (K),[62] 0.0050 M CD_2Cl_2 solutions of Λ-2^{3+} $2Cl^-BAr_f^-$ and Λ-2^{3+} $2I^-BAr_f^-$ were titrated with (*S*)-**4**, (*R*)-**4**, (*S*)-**10**, and (*R*)-**10**. The concentrations of the analytes were plotted *vs.* the change in chemical shift of the C_2 NH protons. The K values were calculated by nonlinear least-square curve fitting using the 1 : 1 stoichiometry established from the Job plots and standard equations and software (Experimental section and Fig. S7 (ESI†)).

As can be seen in Table 4, the alcohol **10** exhibited the lowest K values (7.60–2.73 M^{-1}), while those of the corresponding acetate **4** were somewhat higher (124–22.6 M^{-1}). Whereas (*R*)-**4** gave somewhat higher K values than (*S*)-**4**, (*S*)-**10** (which has the same relative configuration as (*S*)-**4**) gave higher K values than (*R*)-**10**. The K values for Λ-2^{3+} $2I^-BAr_f^-$ and either enantiomer of **4** were considerably higher than those with Λ-2^{3+} $2Cl^-BAr_f^-$.

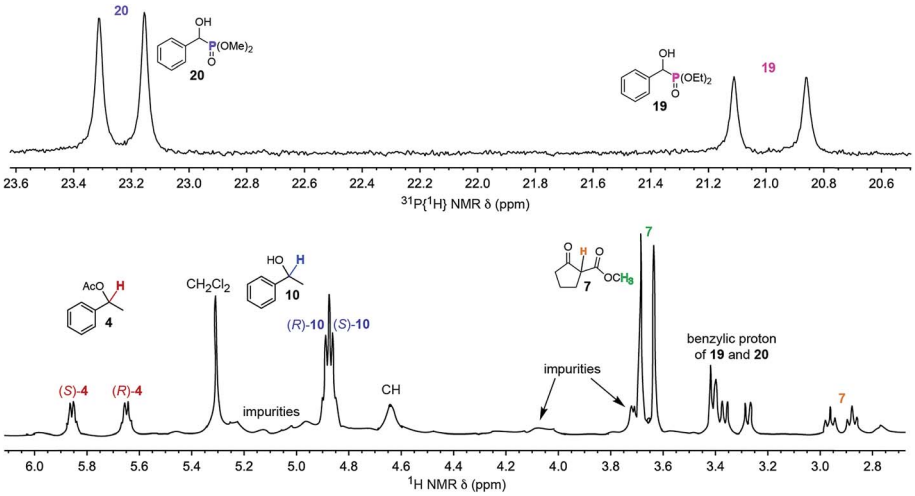

Fig. 4 $^{31}P\{^{1}H\}$ (top) and ^{1}H (bottom) NMR spectra of a $CDCl_3$ solution of a 2.0 : 2.0 : 2.0 : 1.0 : 2.0 : 1.0 mixture of **4**, **7**, **10**, **19**, **20** and the CSA Λ-$\mathbf{2}^{3+}$ $2I^{-}BAr_f^{-}$ (50 mol% *vs.* **4**, **7**, **10**, and **20**; 100 mol% *vs.* **19**).

However, they were much more comparable for the other analytes.

2.7. Crystal structure of a DMSO adduct

Efforts were made to cocrystallize salts of $\mathbf{2}^{3+}$ with analytes from Tables 2 and 3. This proved to be much more challenging than anticipated. Finally, diethyl ether was allowed to vapor diffuse into a DMSO solution of Λ-$\mathbf{2}^{3+}$ $3I^{-}$. This gave yellow blocks of the hexakis(DMSO) solvate Λ-$\mathbf{2}^{3+}$ $3I^{-}\cdot 6$DMSO. X-ray data were acquired and the structure was solved as outlined in Table S3 (ESI†) and the Experimental section. The unit cell contained two independent molecules. Their structures were quite similar, so only one is depicted in Fig. 7.

Although there was no crystallographic symmetry, the trication exhibited an idealized C_3 axis. This lies perpendicular to the plane of the paper in the top view in Fig. 7. Furthermore, three idealized C_2 axes lie in the plane of the paper. The bottom view in Fig. 7 is oriented so that one C_2 axis runs perpendicular to the plane of the paper. Since the CHPh–CHPh bonds of each chelate are parallel to the C_3 axis (Fig. 7, top), the trication is said to exhibit a *lel*$_3$ orientation,[41] as previously found in the crystal structure of Λ-$\mathbf{2}^{3+}$ $3Cl^{-}$ (Fig. 1, bottom).

As illustrated in Fig. S8 (ESI†), two of the three iodide anions hydrogen bond to the three NH groups on opposite C_3 faces, consistent with the rationale for the downfield NH ^{1}H NMR signals in Fig. 5. The I···HN and I···N distances (2.725–2.835 Å (avg 2.767 Å)[63–65] and 3.612–3.712 Å (avg 3.648 Å)) are in typical ranges.[66] The closest contacts for the third iodide anion (see Fig. S9 and S10†) involve the hydrogen atoms of DMSO molecules (2.996–4.043 Å; avg 3.330 Å) and phenyl rings of adjacent trications (3.027–3.285 Å; avg 3.121 Å).[63–65]

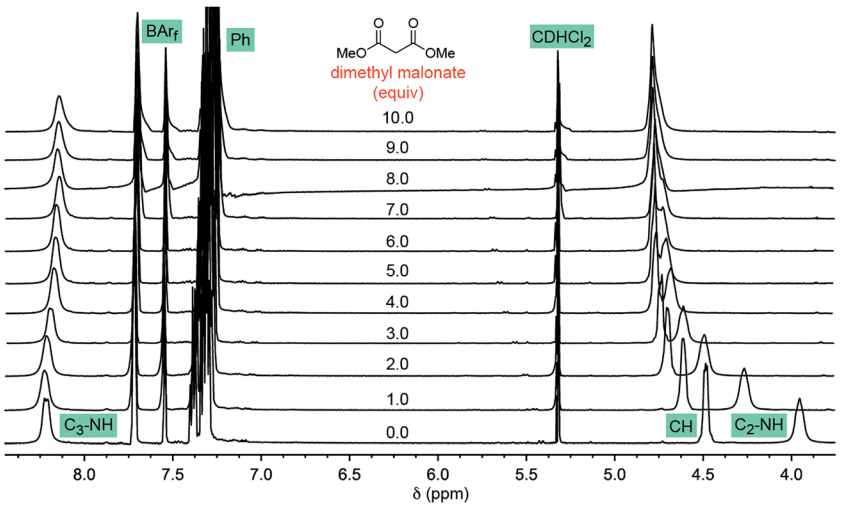

Fig. 5 ^{1}H NMR spectra: titration of a 0.019 M CD_2Cl_2 solution of Λ-$\mathbf{2}^{3+}$ $2Cl^{-}BAr_f^{-}$ (0.0076 mmol; bottom spectrum) with dimethyl malonate in 0.0080 mL (0.0073 mmol) increments (ten ascending spectra).

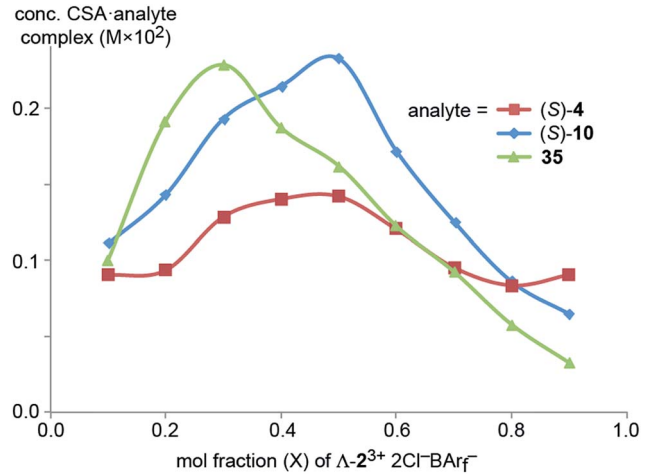

Fig. 6 Job plots for mixtures of Λ-2^{3+} $2Cl^-BAr_f^-$ and (*S*)-1-phenylethyl acetate ((*S*)-**4**), (*S*)-1-phenylethanol ((*S*)-**10**), and DMSO (**35**) in CD_2Cl_2 at ambient temperature.

Table 4 Binding constants (*K*) for CSAs and representative analytes in CD_2Cl_2 at 23 °C

Entry	CSA	analyte	K^a (M^{-1})
1	Λ-2^{3+} $2Cl^-BAr_f^-$	(*S*)-**4**	22.6
2	Λ-2^{3+} $2Cl^-BAr_f^-$	(*R*)-**4**	28.1
3	Λ-2^{3+} $2I^-BAr_f^-$	(*S*)-**4**	104
4	Λ-2^{3+} $2I^-BAr_f^-$	(*R*)-**4**	124
5	Λ-2^{3+} $2Cl^-BAr_f^-$	(*S*)-**10**	7.60
6	Λ-2^{3+} $2Cl^-BAr_f^-$	(*R*)-**10**	2.73
7	Λ-2^{3+} $2I^-BAr_f^-$	(*S*)-**10**	5.60
8	Λ-2^{3+} $2I^-BAr_f^-$	(*R*)-**10**	4.28

[a] See Experimental section including the ESI for details.

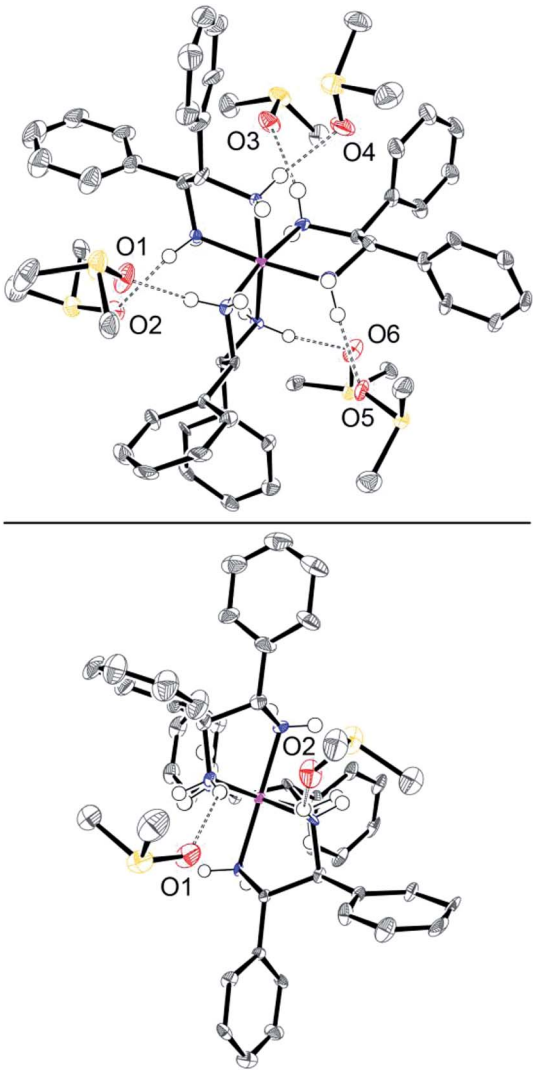

Fig. 7 Thermal ellipsoid diagram (50% probability level) of the trication of Λ-2^{3+} $3I^-\cdot 6$DMSO viewed along the idealized C_3 axis (top) with all six DMSO molecules, and along one of three idealized C_2 axes (bottom) with two DMSO molecules.

As shown in Fig. 7 (top) and Table S4,† the oxygen atoms of all six DMSO molecules make a single hydrogen bond to a different NH group associated with the three C_2 faces. The O···HN and O···N distances (1.975–2.290 Å (avg 2.132 Å)[63–65] and 2.869–3.006 Å (avg 2.929 Å)) are close to those found in other crystallographically characterized adducts of DMSO with NH hydrogen bond donors (for five typical examples[67–71] 1.81–2.10 Å (avg 1.97 Å) and 2.65–2.85 Å (avg 2.77 Å)). For further validation, the sums of the relevant van der Waals radii can be considered (oxygen/hydrogen, 1.52 + 1.20–1.10 Å; oxygen/nitrogen, 1.52 + 1.55 Å).[72–74] The closer contacts in Λ-2^{3+} $3I^-\cdot 6$DMSO confirm bonding interactions by both classical[75] and modern[76] criteria.

Over 150 crystal structures of salts of the trication $[Co(en)_3]^{3+}$ have been determined, and the diverse types of NH/anion hydrogen bonding interactions observed have been reviewed and classified.[45] The bonding motifs exhibited by the two proximal iodide anions in Λ-2^{3+} $3I^-\cdot 6$DMSO are quite common and have been given the designation $[C_3,C_3,C_3][1]$. Those for the DMSO molecules would be abbreviated $[C_2][1]$.

3. Discussion

3.1. New CSAs *vs.* literature systems

The preceding data document an impressive efficacy of Λ-2^{3+} $2Cl^-BAr_f^-$ and Λ-2^{3+} $2I^-BAr_f^-$ as CSAs. The former has the advantage of being commercially available, whereas the latter (easily synthesized from the former) exhibits superior performance characteristics apparently connected to its solubility in $CDCl_3$. The data for Λ-2^{3+} $2Cl^-B(C_6F_5)_4^-$ in Table 1 suggest that salts with related tetraarylborate anions may be comparably effective. The mechanism of action (following section) clearly involves hydrogen bonding between the C_2 NH donor groups of the CSAs and the analytes.

Most of the other CSAs described in the literature also feature hydrogen bond donor groups,[17,19–21,23–30] although many possess acceptor groups as well.[17,20,21,23,29] Typical donor groups include ureas or chalcogenoureas,[25,26,30] squaramides,[27]

secondary amines,[24] amides of primary amines,[17,23,29] sulfonamides,[19] and BINOL derivatives.[20] However, many of these have only been applied to one or two functional groups.

The most broadly applicable CSAs for chirality sensing reported to date have been developed by Ema, Sakai and coworkers.[17] Their lead system, **48** (Fig. 8), was applied to ten functional groups, three of which were not assayed with Λ-2^{3+} $2X^-BAr_f^-$ (oxazolidinone, sulfoximine, isocyanate). Their typical loadings were 100–200 mol%, although a chiral sulfoxide was found to require only 5 mol%. Conversely, Tables 2 and 3 contain several functional groups that they did not study (ester/β-ketoester, amine, amide/sulfonamide, hydroxyphosphonate, ketone/1,3-diketone, ether). Furthermore, with our lead CSA, Λ-2^{3+} $2I^-BAr_f^-$, the average loading is 14% (range 1–100%).

There is a wider selection of CSAs that have been applied to four-seven functional groups.[21,22,25,29] These generally require loadings of 100–300 mol%, although with one analyte the CSA **49** (Fig. 5, R = Ph) was shown to be effective at 60 mol%. None of these CSAs are commercially available. However, another group has assembled a library of 32 commercial CSAs, and developed high throughput protocols for identifying optimal partners for specific analytes.[77] Far fewer CSAs have been applied to prochirality sensing, and the eight functional groups represented in Table 3 exceed the sum of all those in the literature we have been able to locate.[48–54]

To our knowledge, the above salts of Λ-2^{3+} represent the first CSAs that are based upon transition metals. However, transition metals are well represented among chiral derivatizing agents (CDAs).[61,78,79] The salt **49** (ref. 22) in Fig. 8 is based upon a main group metal, aluminum, and displays several conceptual similarities with our cobalt(III) systems. First, both metals are octahedral and constitute stereocenters. Second, the anion of **49** has C_2 symmetry, *vs.* D_3 symmetry for the trication 2^{3+}. Third, **49** has two Al–NH groups that can serve as hydrogen bond donors (as well as four Al–O groups that can serve as hydrogen bond acceptors).

3.2. Analyte binding to Λ-2^{3+}

There is a variety of evidence that the enthalpy of hydrogen bonding to a C_3 face of Λ-2^{3+} (**A**, Fig. 1) is much greater than that to a C_2 face (**B**, Fig. 1). For example, the solid state structures of the diastereomeric trichloride salts Λ- and Δ-2^{3+} $3Cl^-$ show the three chloride ions to be distributed over two C_3 faces and one C_2 face (as opposed to, for example, three C_2 faces).[37] Scheme 1 shows that one chloride ion – presumably that associated with the C_2 face – can more easily be replaced by the very poor hydrogen bond acceptor BAr_f^- than the other two.[37,42] As illustrated by the bottom trace in Fig. 5, the ^{1}H NMR spectra of mixed salts Λ-2^{3+} $2X^-BAr_f^-$ always show two NH signals of equal area (6H/6H), with the downfield signal moving upfield as X^- becomes a poorer hydrogen bond acceptor (*e.g.*, BF_4^-, PF_6^-).[37,42] These observations are consistent with two "occupied" C_3 faces and three "free" C_2 faces.

When Λ-2^{3+} $2Cl^-BAr_f^-$ is titrated with suitable substrates, such as dimethyl malonate in Fig. 5, the upfield NH groups shift markedly downfield, but the downfield NH groups are much less affected. This indicates dominant analyte binding at the C_2 faces. In accord with the Job plots (Fig. 6), we presume that the binding constants for the first one ((*S*)-**4**, (*S*)-**10**) or two (**35**) analyte molecules are much greater than those for additional molecules. This may seem at odds with the crystal structure in Fig. 7, in which the three C_2 faces engage in hydrogen bonding with six DMSO molecules (one per NH group). However, interactions that may be very weak in solution are often expressed in the solid state, where physical packing effects may also play roles. For example, one could speculate that a crystal lattice grows faster when comprised of more symmetrical entities derived from six-fold DMSO binding.

The binding constants (K) in Table 4 track the order found for the hydrogen bond donor *p*-fluorophenol and the analytes ethyl acetate and benzyl alcohol (CCl_4, 25 °C; 11.7 and 7.24 M^{-1}).[80] Those for the acetate **4** (22–124 M^{-1}) are in the range of values measured for other CSAs and cyclic esters,[17,19] and those for the benzylic alcohol **10** (2.7–7.6 M^{-1}) likewise compare well with values obtained with other benzylic alcohols.[26]

The loss of efficacy of Λ-2^{3+} $2Cl^-BAr_f^-$ and Λ-2^{3+} $2I^-BAr_f^-$ in coordinating solvents (entries 8–13, Table 1) presumably reflects the saturation of the C_2 faces, obstructing access by the analytes. The halide free salt Λ-2^{3+} $3BAr_f^-$, with three very poorly hydrogen bond accepting anions, gives much lower Δδ values (entry 5, Table 1). We speculate that the analyte now preferentially binds to an "unoccupied" C_3 face, which for some reason gives diminished chiral recognition. Naturally, the cocrystallization of additional analytes with all of the preceding cobalt(III) complexes remains a goal. Crystal structures have been reported for analyte adducts of only a few other CSAs.[22,24] Alternatively, insight can be gained by computational studies,[22,23,26–28] and a series of DFT investigations are currently underway.

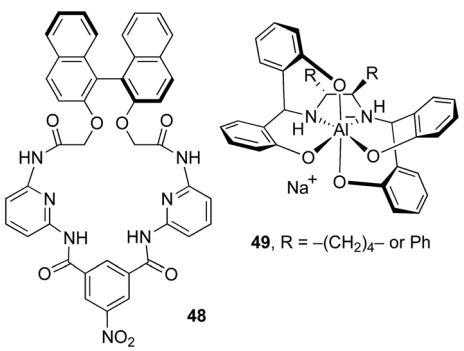

Fig. 8 Some relevant previously reported CSAs.

3.3. Conclusion

The new cobalt based CSAs described above offer unparalleled functional group applicability, effectiveness at significantly lower loadings and in the presence of multiple analytes, extended stability to air and water, and ready availability from inexpensive building blocks. Their success reflects the

generality of second coordination sphere hydrogen bonding between the NH donor groups and Lewis basic functional groups in the analytes. Given the many "best in class" characteristics, and recent commercial availability,[47] they appear primed for wide adoption.

4. Experimental section

4.1. General

The CSAs Λ-2^{3+} $2Cl^-BAr_f^-$, Λ-2^{3+} $2Cl^-B(C_6F_5)_4^-$, Λ-2^{3+} $3BAr_f^-$, and Δ-2^{3+} $2Cl^-BAr_f^-$ were synthesized as reported earlier,[42] and Λ-1^{3+} $3BAr_f^-$ was prepared as described for the enantiomer;[36] Λ-2^{3+} $2Cl^-BAr_f^-$ is also commercially available.[47] All abbreviations are defined in the introduction. All reactions and workups were conducted in air.

4.2. Λ-2^{3+} $3I^-$

A round bottom flask was charged with a suspension of Λ-2^{3+} $3Cl^-\cdot 3H_2O$ (0.170 g, 0.199 mmol)[42] in acetone (20 mL) and KI (0.099 g, 0.597 mmol) was added with vigorous stirring. A suspension of white particles in an orange solution formed. After 1 h, the mixture was filtered. The solvent was removed from the filtrate by rotary evaporation and oil pump vacuum (20 h, rt) to give Λ-2^{3+} $3I^-\cdot 3H_2O$ (0.219 g, 0.194 mmol, 97%) as an orange solid, mp 200–202 °C dec (open capillary). Anal. calcd for $C_{42}H_{48}CoI_3N_6\cdot 3H_2O$ (1130.07): C 44.62, H 4.81, N 7.43; found C 44.81, H 4.91, N 7.02.

NMR (CD_3OD/acetone-d_6, δ in ppm): ^{1}H (500 MHz) 7.51–7.49 (m, 12H, *o*-Ph), 7.38–7.37 (m, 18H, *m*-, *p*-Ph), 6.75 (br s, 6H, N**H**H′), 5.95 (br s, 6H, NH**H**′), 5.26 (s, 6H, C**H**Ph), 2.83 (br s, 7H, **H**$_2$O); ^{13}C{^{1}H} (125 MHz) 136.4 (s, *i*-Ph), 130.1 (s, *p*-Ph), 129.9 and 129.7 (2 s, *o*- and *m*-Ph), 62.8 (s, **C**HPh). IR (powder film, cm^{-1}): 3032 (m, ν_{NH}), 1683 (m, δ_{NH}), 1041 (vs, δ_{CCN}).

4.3. Λ-2^{3+} $2I^-BAr_f^-$

A. A round bottom flask was charged with Λ-2^{3+} $3I^-\cdot 3H_2O$ (0.117 g, 0.104 mmol), CH_2Cl_2 (20 mL), H_2O (20 mL), and Na^+ BAr_f^- (0.092 g, 0.104 mmol). The mixture was vigorously stirred until the orange color had entirely transferred to the CH_2Cl_2 layer (30 min), which was separated. The solvent was removed by passive evaporation (fume hood) and oil pump vacuum (20 h, rt) to give Λ-2^{3+} $2I^-BAr_f^-\cdot 0.5H_2O$ (0.188 g, 0.103 mmol, 99%) as a red solid, mp 107–110 °C dec (black liquid, open capillary). Anal. calcd for $C_{74}H_{60}BCoF_{24}I_2N_6\cdot 0.5H_2O$ (1821.20): C 48.79, H 3.37, N 4.61; found C 48.88, H 3.61, N 4.62. **B.** A round bottom flask was charged with aqueous NaI (15.0 mL, 10 wt%, 10.5 mmol), toluene (15.0 mL), and Λ-2^{3+} $2Cl^-BAr_f^-\cdot 2H_2O$ (0.259 g, 0.152 mmol). The mixture was vigorously stirred, and after 6 h transferred to a separatory funnel. The clear aqueous layer was discarded and the red toluene layer was washed with water (2 × 10 mL). The solvent was removed from the toluene layer by rotary evaporation. The residue was dissolved in CH_3OH (10 mL) and the solution was stirred for 20 min.[81] The solvent was removed again by rotary evaporation and oil pump vacuum (10 h, rt) to give Λ-2^{3+} $2I^-BAr_f^-\cdot 0.5H_2O$ (0.277 g, 0.152 mmol, >99%) as a red solid, mp 108–110 °C dec (black liquid, open capillary). Anal. calcd, see above; found C 49.17, H 3.50, N 4.46.

Data for Λ-2^{3+} $2I^-BAr_f^-\cdot 0.5H_2O$. NMR (δ in ppm): ^{1}H (500 MHz, $CDCl_3$ or CD_2Cl_2) BAr_f^- at 7.69 or 7.71 (s, 8H, *o*), 7.49 or 7.55 (s, 4H, *p*); (*S*,*S*)-dpen at 7.37–7.27 or 7.44−7.29 (m, 30H, Ar**H**), 6.98 or 7.88 (br s, 6H, N**H**H′), 4.86 or 4.21 (br s, 6H, NH**H**′), 4.60 (s, 6H, C**H**Ph); 2.22 or 1.78 (br s, 5H or 2H, **H**$_2$O).[82] ^{13}C{^{1}H} (126 MHz, CD_2Cl_2) BAr_f^- at 162.3 (q, $^1J_{BC}$ = 49.8 Hz, i), 135.4 (s, *o*), 129.4 (q, $^2J_{CF}$ = 31.5 Hz, *m*), 125.2 (q, $^1J_{CF}$ = 272.3 Hz, CF_3), 118.1 (s, *p*); (*S*,*S*)-dpen ligand at 134.6 (s, i-Ph), 130.8 (s, *p*-Ph), 130.3 (s, *o*-Ph), 128.7 (s, *m*-Ph), 62.7 (s, **C**HPh). IR (powder film, cm^{-1}): 3064 (m, ν_{NH}), 1608 (m, δ_{NH}), 1354 (s, $\nu_{Ar\text{-}CF_3}$), 1275 (vs, ν_{CF}), 1117 (vs, δ_{CCN}).

4.4. Dependence of Δδ upon CSA and solvent (Table 1)

A 5 mm NMR tube was charged with a 0.0071 M solution of a CSA (0.70 mL, 0.0049 mmol) in the indicated solvent. Neat 1-phenylethyl acetate (**4**; 0.00050 mL, 0.0012 g, 0.0050 mmol) was added and a ^{1}H NMR spectrum was recorded.

4.5. Dependence of Δδ upon mol% of CSA (Fig. 2)

A 5 mm NMR tube was charged with a CD_2Cl_2 solution of Λ-2^{3+} $2Cl^-BAr_f^-\cdot 2H_2O$ (0.70 mL, 0.036 M, 0.025 mmol). Neat **4** was then added in 0.00050 mL increments (*ca.* 0.0012 g, 0.0050 mmol). A ^{1}H NMR spectrum was acquired after each addition. The total volume of **4** added from the first data point (500 mol%) to the final data point (5 mol%) was 0.050 mL.

4.6. Dependence of Δδ upon concentration (Fig. 3)

A 5 mm NMR tube was charged with a CD_2Cl_2 solution (0.50 mL) that was 0.040 M in **4** (0.020 mmol) and 0.010 M in Λ-2^{3+} $2Cl^-BAr_f^-\cdot 2H_2O$ (0.0050 mmol, 25 mol%). A ^{1}H NMR spectrum was recorded. Then CD_2Cl_2 was added in increments so as to attain total volumes of 0.60, 0.70, 0.80, 0.90, 1.00, 1.10, 1.50, 2.00, 3.00, 4.00, and 5.00 mL. After each addition, a ^{1}H NMR spectrum was recorded.

4.7. Chirality sensing (Table 2)

A (liquid analytes **4–7**, **10**, **14–18**, **21–25**, **27–29**, **31**). 5 mm NMR tubes were charged with CD_2Cl_2 solutions of Λ-2^{3+} $2Cl^-BAr_f^-\cdot 2H_2O$ or $CDCl_3$ solutions of Λ-2^{3+} $2I^-BAr_f^-\cdot 0.5H_2O$ (0.70 mL, 0.0071 M, 0.0049 mmol). The samples were titrated with neat liquid analytes in increments of 0.0050 mmol (1.0 equiv.) and monitored by ^{1}H NMR. Experiments were halted when separate signals for the enantiomers were no longer observed. The total volume of liquids added usually ranged from 0.72 to 0.80 mL. **B** (solid analytes **8**, **9**, **11–13**, **19–20**, **26**, **30**). Procedure A was repeated, but with the analytes added as 10.0 M CD_2Cl_2 or $CDCl_3$ solutions in increments of 0.00050 mL (0.0050 mmol).

4.8. Enhanced throughput sensing (Fig. 4)

A 5 mm NMR tube was charged with a $CDCl_3$ solution (0.70 mL) that was 0.029 M in **4**, **7**, **10**, and **20** (0.020 mmol each), and 0.014 M in **19** (0.010 mmol). Then Λ-2^{3+} $2I^-BAr_f^-\cdot 0.5H_2O$

(0.018 g, 0.010 mmol) was added, and ^{1}H and ^{31}P{^{1}H} NMR spectra were recorded.

4.9. Prochirality sensing (Table 3)

A 5 mm NMR tube was charged with a CD_2Cl_2 solution of Λ-2^{3+} $2Cl^-BAr_f^-\cdot 2H_2O$ or a $CDCl_3$ solution of Λ-2^{3+} $2I^-BAr_f^-\cdot 0.5H_2O$ (0.70 mL, 0.0071 M, 0.0049 mmol). The analyte (1.0 equiv.) was added as a neat liquid (**32–38**, **40–42**, **44**, **46**) or solid (**39**, **43**, **45**, **47**) and ^{1}H NMR spectra were recorded.

4.10. Titration of a CSA with dimethyl malonate (Fig. 5)

A 5 mm NMR tube was charged with a 0.019 M CD_2Cl_2 solution (0.40 mL) of Λ-2^{3+} $2Cl^-BAr_f^-\cdot 2H_2O$ (0.0076 mmol). A reference ^{1}H NMR spectrum were recorded. A 0.91 M CD_2Cl_2 solution of dimethyl malonates was added in 0.0080 mL increments (0.0073 mmol). A ^{1}H NMR spectrum was recorded after each addition.

4.11. Job plots (Fig. 6)[62]

0.010 M CD_2Cl_2 solutions of Λ-2^{3+} $2Cl^-BAr_f^-\cdot 2H_2O$ and (*S*)-**4** were prepared and mixed at nine volume ratios (mL/mL: 0.050/0.45, 0.10/0.40, 0.15/0.35, 0.20/0.30, 0.25/0.25, 0.30/0.20, 0.35/0.15, 0.40/0.10, 0.45/0.050). ^{1}H NMR spectra were recorded (500 MHz) and the concentration of the adduct CSA·(*S*)-**4** calculated from the equation[83,84]

$$[\text{CSA}\cdot(S)\text{-}\mathbf{4}] = [(\delta_{obs} - \delta_0)/(\delta_c - \delta_0)] \times [\text{CSA}]$$

where [CSA] is the concentration of Λ-2^{3+} $2Cl^-BAr_f^-$ in the sample, δ_{obs} is the chemical shift of the C_2 NH protons in the sample (always upfield from the C_3 NH protons),[42] δ_0 is the chemical shift of the C_2 NH protons of Λ-2^{3+} $2Cl^-BAr_f^-$ in otherwise identical samples that lack (*S*)-**4**, and δ_c is the chemical shift of the C_2 NH protons in the complex CSA·(*S*)-**4**. The values for [CSA·(*S*)-**4**] were then plotted *versus* the mol fraction (*X*) of Λ-2^{3+} $2Cl^-BAr_f^-$ per Fig. 6. This procedure was repeated with 0.010 M CD_2Cl_2 solutions of Λ-2^{3+} $2Cl^-BAr_f^-$ and (*S*)-**10** or **35**.

4.12. Binding constants (Table 4)[62]

0.0050 M CD_2Cl_2 solutions of Λ-2^{3+} $2Cl^-BAr_f^-\cdot 2H_2O$ and Λ-2^{3+} $2I^-BAr_f^-\cdot 0.5H_2O$ were prepared. One 5 mm NMR tube was charged with 1.0 mL of one solution, and another tube with 1.0 mL of the other. Reference ^{1}H NMR spectra were recorded. Analytes were then added in 0.0050 mmol increments (1.0 equiv.) using a microsyringe, and a ^{1}H NMR spectrum was recorded after each addition. The concentrations of the analytes were plotted *versus* the change in chemical shift of the C_2 NH protons ($\Delta\delta = \delta_{obs} - \delta_0$) as in Fig. S7.† The binding constants *K* were calculated by nonlinear least-square curve fitting using Origin Pro 8.0,[85] the 1 : 1 stoichiometry established from the Job plots, and the equation[86]

$$[\text{Analyte}] = (1/K) \times [x/(1 - x)]$$

where $x = (\delta_{obs} - \delta_0)/(\delta_c - \delta_0)$.

4.13. Crystallography

A solution of Λ-2^{3+} $3I^-\cdot 3H_2O$ (0.011 g, 0.010 mmol) in DMSO (0.50 mL) in an open vial was placed inside a 20 mL closed vial containing diethyl ether (7.0 mL). After 4 d, yellow blocks were collected. Data were obtained as outlined in Table S3.† Cell parameters were determined from 45 data frames using a 1° scan. Integrated intensity information for each reflection was obtained by reduction of the data frames with the program APEX3.[87] Data were corrected for Lorentz, polarization, and crystal decay effects. SADABS[88] was employed for absorption corrections, and the structure was solved using XT/XS in APEX3.[87,89–92] The unit cell contained two independent molecules of Λ-2^{3+} $3I^-$, each associated with six molecules of DMSO. Hydrogen atoms were placed in idealized positions and refined using a riding model. All non-hydrogen atoms were refined with anisotropic thermal parameters. Five of the DMSO molecules were disordered over two positions (occupancy ratios: C1S/3A, C1R/4A, O2/2A, S2/2A, 72 : 28; C1T/6A, C1U/5A, O3/3A, S3/3A, 79 : 21; C1V/8A, C1W/7A, O4/4A, S4/4A, 78 : 22; C1X/10A, C1Y/9A, O5/5A, S5/5A, 72 : 28; C2C/2E, C1AA/2CA, O12/12A, S12/12A, 52 : 48). Restraints were applied to keep the metrical parameters meaningful. The data were refined by weighted least squares refinement on F^2 to convergence.[89–93] PLATON (ADDSYM)[94] was used to verify the absence of additional symmetry and voids. Flack's parameter (Table S3†) confirmed the absolute stereochemistry.[95]

Conflicts of interest

The authors have a financial interest in the CSAs described in this work, some of which are commercially available.[47]

Acknowledgements

The authors thank the Welch Foundation (Grant A-1656) for support.

References

1 P. Schreier, A. Bernreuther and M. Huffer, *Analysis of Chiral Organic Molecules: Methodology and Applications*, Walter de Gruyter & Co., Berlin, Germany, 1995.
2 G. G. Lyle and R. E. Lyle, in *Asymmetric Synthesis*, ed. J. D. Morrison, Academic Press, Inc., New York, NY, 1983, vol. 1, ch. 2, pp. 13–27.
3 V. Schurig, in *Asymmetric Synthesis*, ed. J. D. Morrison, Academic Press, Inc., New York, 1983, vol. 1, ch. 5, pp. 59–60.
4 D. Leung, S. O. Kang and E. V. Anslyn, *Chem. Soc. Rev.*, 2012, **41**, 448–479, and ref. 4 and 6–10 therein.
5 H. H. Jo, C.-Y. Lin and E. V. Anslyn, *Acc. Chem. Res.*, 2014, **47**, 2212–2221 and ref. 12 therein.
6 V. Schurig, *J. Chromatogr. A*, 2001, **906**, 275–299.
7 Y. Okamoto and T. Ikai, *Chem. Soc. Rev.*, 2008, **37**, 2593–2608.
8 T. J. Wenzel, *Discrimination of Chiral Compounds Using NMR Spectroscopy*, John Wiley & Sons, Hoboken, NJ, 2007.

9 T. J. Wenzel, in *Differentiation of Enantiomers II*, ed. V. Schurig, Springer-Verlag, Berlin, Germany, 2013, ch. 1, pp. 1–68.
10 T. J. Wenzel and C. D. Chisholm, *Chirality*, 2011, **23**, 190–214.
11 T. J. Wenzel and C. D. Chisholm, *Prog. Nucl. Magn. Reson. Spectrosc.*, 2011, **59**, 1–63.
12 M. S. Silva, *Molecules*, 2017, **22**, 247.
13 G. Uccello-Barretta and F. Balzano, in *Differentiation of Enantiomers II*, ed. V. Schurig, Springer-Verlag, Berlin, Germany, 2013, ch. 2, pp. 69–132.
14 M. Raban and K. Mislow, *Tetrahedron Lett.*, 1965, **6**, 4249–4253.
15 J. A. Dale, D. L. Dull and H. S. Mosher, *J. Org. Chem.*, 1969, **34**, 2543–2549.
16 S.-I. Aizawa, M. Okano and T. Kidani, *Chirality*, 2017, **29**, 273–281 and ref. 1–29 therein.
17 T. Ema, D. Tanida and T. Sakai, *J. Am. Chem. Soc.*, 2007, **129**, 10591–10596.
18 Representative papers that have appeared since 2014 and describe new CSAs are given in ref. 19–30. For a complete bibliography for this period, see the additional ref. S14–S29 (ESI†).
19 A. Couffin, O. Thillaye du Boullay, M. Vedrenne, C. Navarro, B. Martin-Vaca and D. Bourissou, *Chem. Commun.*, 2014, **50**, 5997–6000.
20 I. Pal, S. R. Chaudhari and N. Suryaprakash, *New J. Chem.*, 2014, **38**, 4908–4912.
21 A. Lakshmipriya, S. R. Chaudhari and N. Suryaprakash, *Chem. Commun.*, 2015, **51**, 13492–13495.
22 M.-S. Seo and H. Kim, *J. Am. Chem. Soc.*, 2015, **137**, 14190–14195.
23 H. Huang, G. Bian, H. Zong, Y. Wang, S. Yang, H. Yue, L. Song and H. Fan, *Org. Lett.*, 2016, **18**, 2524–2527.
24 R. Gupta, R. G. Gonnade and A. V. Bedekar, *J. Org. Chem.*, 2016, **81**, 7384–7392.
25 G. Bian, S. Yang, H. Huang, H. Zong and L. Song, *Sens. Actuators, B*, 2016, **231**, 129–134.
26 G. Bian, S. Yang, H. Huang, H. Zong, L. Song, H. Fan and X. Sun, *Chem. Sci.*, 2016, **7**, 932–938.
27 Y. Li, G.-H. Yang, C. Q. He, X. Li, K. N. Houk and J.-P. Cheng, *Org. Lett.*, 2017, **19**, 4191–4194.
28 C. Lv, L. Feng, H. Zhao, G. Wang, P. Stavropoulos and L. Ai, *Org. Biomol. Chem.*, 2017, **15**, 1642–1650.
29 N. Jain, A. N. Khanvilkar, S. Sahoo and A. Bedekar, *Tetrahedron*, 2018, **74**, 68–76.
30 S. Ito, M. Okuno and M. Asami, *Org. Biomol. Chem.*, 2018, **16**, 213–222.
31 A. Werner, *Chem. Ber.*, 1912, **45**, 121–130.
32 A. Werner, *Chem. Ber.*, 1911, **44**, 3279–3284.
33 A. Werner, *Chem. Ber.*, 1911, **44**, 3272–3278.
34 A. Werner, *Chem. Ber.*, 1911, **44**, 2445–2455.
35 A. Werner, *Chem. Ber.*, 1911, **44**, 1887–1898. V. L. King is listed as an author for the Experimental section.
36 C. Ganzmann and J. A. Gladysz, *Chem.–Eur. J.*, 2008, **14**, 5397–5400.
37 K. G. Lewis, S. K. Ghosh, N. Bhuvanesh and J. A. Gladysz, *ACS Cent. Sci.*, 2015, **1**, 50–56.
38 A. Kumar, S. K. Ghosh and J. A. Gladysz, *Org. Lett.*, 2016, **18**, 760–763.
39 H. Joshi, S. K. Ghosh and J. A. Gladysz, *Synthesis*, 2017, **49**, 3905–3915.
40 S. K. Ghosh, C. Ganzmann, N. Bhuvanesh and J. A. Gladysz, *Angew. Chem., Int. Ed.*, 2016, **55**, 4356–4360; *Angew. Chem.*, 2016, **128**, 4429–4433.
41 Review of stereoisomerism in salts of the trication $[Co(en)_3]^{3+}$, and homologs with substituted 1,2-diamine ligands: A. Ehnbom, S. K. Ghosh, K. G. Lewis and J. A. Gladysz, *Chem. Soc. Rev.*, 2016, **45**, 6799–6811.
42 S. K. Ghosh, K. G. Lewis, A. Kumar and J. A. Gladysz, *Inorg. Chem.*, 2017, **56**, 2304–2320.
43 S. K. Ghosh, C. Ganzmann and J. A. Gladysz, *Tetrahedron: Asymmetry*, 2015, **26**, 1273–1280.
44 The best prices in effect as of the submission date of this manuscript are from Oakwood Chemical (http://www.oakwoodchemical.com) (*R*,*R*-dpen; $359/100 g) and Ark Pharm (http://www.arkpharminc.com) (*S*,*S*-dpen; $420/100 g). Accessed 13 February 2018.
45 S. K. Ghosh, A. Ehnbom, K. G. Lewis and J. A. Gladysz, *Coord. Chem. Rev.*, 2017, **350**, 30–48.
46 H. Miyabe and Y. Takemoto, *Bull. Chem. Soc. Jpn.*, 2008, **81**, 785–795.
47 https://secure.strem.com/catalog/v/27–4010/16/cobalt_1542135-29-4, accessed 13 February 2018.
48 For a brief review of the differentiation of enantiotopic (prochiral) groups by NMR, see pp. 339–341 of ref. 8. For prochirality sensing using CSAs, see ref. 49–54. For prochirality sensing using CLSAs and CDAs, see ref. S30 and S31.† For prochirality sensing using chiral liquid crystals and other chiral media see ref. 55 and S32–S35.†
49 M. J. P. Harger, *J. Chem. Soc., Perkin Trans. 2*, 1980, 1505–1511.
50 F. A. L. Anet and J. Park, *J. Am. Chem. Soc.*, 1992, **114**, 411–416.
51 M. T. Reetz, J. Rudolph and R. Mynott, *J. Am. Chem. Soc.*, 1996, **118**, 4494–4495.
52 A. Bilz, T. Stork and G. Helmchen, *Tetrahedron: Asymmetry*, 1997, **8**, 3999–4002.
53 Y. Kobayashi, N. Hayashi and Y. Kishi, *Org. Lett.*, 2002, **4**, 411–414.
54 N. Seri, S. Simaan, M. Botoshansky, M. Kaftory and S. Biali, *J. Org. Chem.*, 2003, **68**, 7140–7142.
55 P. Lesot, C. Aroulanda, H. Zimmermann and Z. Luz, *Chem. Soc. Rev.*, 2015, **44**, 2330–2375.
56 All cobalt(III) complexes are isolated as hydrates, consistent with the appreciable hydrogen bond donor strengths of the NH groups. To aid readability, these are not specified in the formulae in the main text or graphics, but are given in the Experimental section. The additional mass is taken into account in the stoichiometries and yield calculations. For additional related remarks, see ref. 23 in ref. 42.
57 J. M. Keith, J. F. Larrow and E. N. Jacobsen, *Adv. Synth. Catal.*, 2001, **343**, 5–26.

58 E. Vedejs and M. Jure, *Angew. Chem., Int. Ed.*, 2005, **44**, 3974–4001; *Angew. Chem.*, 2005, **117**, 4040–4069.
59 H. Pellissier, *Adv. Synth. Catal.*, 2011, **353**, 1613–1666.
60 C. E. Müller and P. R. Schreiner, *Angew. Chem., Int. Ed.*, 2011, **50**, 6012–6042; *Angew. Chem.*, 2011, **123**, 6136–6167.
61 Y. Zhao and T. M. Swager, *J. Am. Chem. Soc.*, 2015, **137**, 3221–3224.
62 K. A. Connors, in *Binding Constants: the Measurement of Molecular Complex Stability*, John Wiley & Sons, New York, NY, 1987, ch. 2, pp. 21–101.
63 The C–H and N–H bond lengths determined from X-ray crystal structures are usually *ca.* 10% too short. See, *inter alia*, ref. 64 and 65.
64 F. H. Allen, *Acta Crystallogr. Sect. B Struct. Sci.*, 1986, **42**, 515–522.
65 B. Dittrich, J. Lübben, S. Mebs, A. Wagner, P. Luger and R. Flaig, *Chem.–Eur. J.*, 2017, **23**, 4605–4614.
66 T. Steiner, *Acta Crystallogr. Sect. B Struct. Sci.*, 1998, **54**, 456–463.
67 J. Mizuguchi, *Acta Crystallogr., Sect. C: Struct. Chem.*, 1992, **48**, 1279–1283.
68 N. Nagel, C. Näther and H. Bock, *Acta Crystallogr., Sect. C: Struct. Chem.*, 1995, **C51**, 1935–1937.
69 K. Wijaya, O. Moers, A. Blaschette and P. G. Jones, *Acta Crystallogr., Sect. C: Struct. Chem.*, 1998, **54**, 1707–1710.
70 R. D. Gilardi and R. J. Butcher, *Acta Crystallogr., Sect. E: Crystallogr. Commun.*, 2001, **57**, o757–o759.
71 A. D. Bond, *Acta Crystallogr., Sect. B: Struct. Sci.*, 2002, **58**, o194–o195.
72 A. Bondi, *J. Phys. Chem.*, 1964, **68**, 441–451.
73 M. Mantina, A. C. Chamberlin, R. Valero, C. J. Cramer and D. G. Truhlar, *J. Phys. Chem. A*, 2009, **113**, 5806–5812.
74 R. S. Rowland and R. Taylor, *J. Phys. Chem.*, 1996, **100**, 7384–7391.
75 W. C. Hamilton and J. A. Ibers, *Hydrogen bonding in solids: methods of molecular structure determination*, ed. W. A. Benjamin, New York, NY, 1968, pp. 14–16.
76 T. Steiner, *Angew. Chem., Int. Ed.*, 2002, **41**, 48–76; *Angew. Chem.*, 2002, **114**, 50–80. See ref. 21 therein for a critique of classical van der Waals criteria.
77 L. Yang, T. Wenzel, R. T. Williamson, M. Christensen, W. Schafer and C. J. Welch, *ACS Cent. Sci.*, 2016, **2**, 332–340.
78 See pp. 365–398 of ref. 8.
79 G. Storch, M. Siebert, F. Rominger and O. Trapp, *Chem. Commun.*, 2015, **51**, 15665–15668.
80 C. Laurence and J.-F. Gal, in *Lewis Basicity and Affinity Scales: Data and Measurement*, John Wiley & Sons, Chichester, UK, 2010, pp. 142–147, and 151.
81 When the CH_3OH treatment was omitted, the toluene solvate Λ-$\mathbf{2}^{3+}$ $2I^-BAr_f^-\cdot 0.8C_7H_8$ was isolated, mp 110–112 °C dec (black liquid, open capillary). Anal. calcd for $C_{74}H_{60}BCoF_{24}I_2N_6\cdot 0.8C_7H_8$ (1885.85): C 50.68, H 3.55, N 4.45; found C 50.09, H 3.63, N 4.38. ^{1}H NMR (500 MHz, CD_2Cl_2, δ in ppm) BAr_f^- at 7.71 (s, 8H, *o*), 7.54 (s, 4H, *p*); (*S*,*S*)-dpen at 7.29–7.45 (m, 30H, Ar**H**), 5.31 (br s, 6H, N**H**H′; partial overlap, $CDHCl_2$), 4.88 (br s, 6H, NH**H**′), 4.69 (s, 6H, C**H**Ph); 2.01 (br s, 18H, $\mathbf{H}_2O$);[82] toluene at 7.15-7.23 (m, 4H, C_6H_5), 2.33 (s, 2.4H, C$\mathbf{H}_3$).
82 The increased level of water over that derived from the microanalysis is believed to originate from the solvent.
83 See pp. 24–28 of ref. 62.
84 P. Thordarson, *Chem. Soc. Rev.*, 2011, **40**, 1305–1323.
85 http://www.originlab.com/.
86 See pp. 189–194 of ref. 62.
87 *APEX3, Program for Data Collection on Area Detectors*, BRUKER AXS Inc., 5465 East Cheryl Parkway, Madison, WI, USA, pp. 53711–5373.
88 G. M. Sheldrick, *SADABS, Program for Absorption Correction of Area Detector Frames*, BRUKER AXS Inc., 5465 East Cheryl Parkway, Madison, WI, USA, pp. 53711–5373.
89 G. M. Sheldrick, *Acta Crystallogr., Sect. A: Found. Adv.*, 2008, **64**, 112–122.
90 G. M. Sheldrick, *Acta Crystallogr., Sect. A: Found. Adv.*, 2015, **71**, 3–8.
91 G. M. Sheldrick, *Acta Crystallogr., Sect. C: Struct. Chem.*, 2015, **71**, 3–8.
92 *X. T, X. S.*, BRUKER AXS Inc., 5465 East Cheryl Parkway, Madison, WI, USA, pp. 53711–5373.
93 O. V. Dolomanov, L. J. Bourhis, R. J. Gildea, J. A. K. Howard and H. Puschmann, *J. Appl. Crystallogr.*, 2009, **42**, 339–341.
94 A. L. Spek, *J. Appl. Crystallogr.*, 2003, **36**, 7–13.
95 H. D. Flack, *J. Appl. Crystallogr.*, 1983, **39**, 876–881. Theory for correct and inverted structures: 0 and 1.